

Series Editor
Gilles Pijaudier-Cabot

Crystal Elasticity

Pascal Gadaud

Color Section

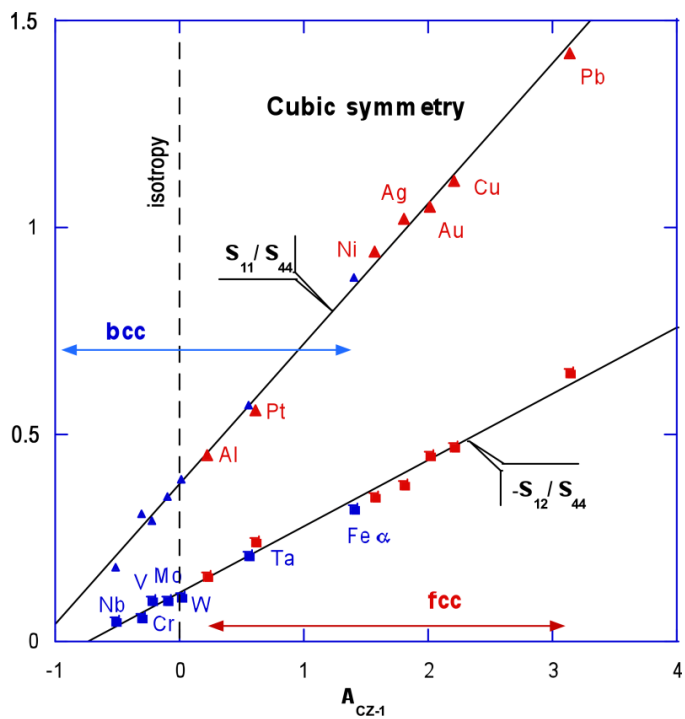


Figure 2.1. *Dimensionless representation of the elasticity of fcc and cc metals*

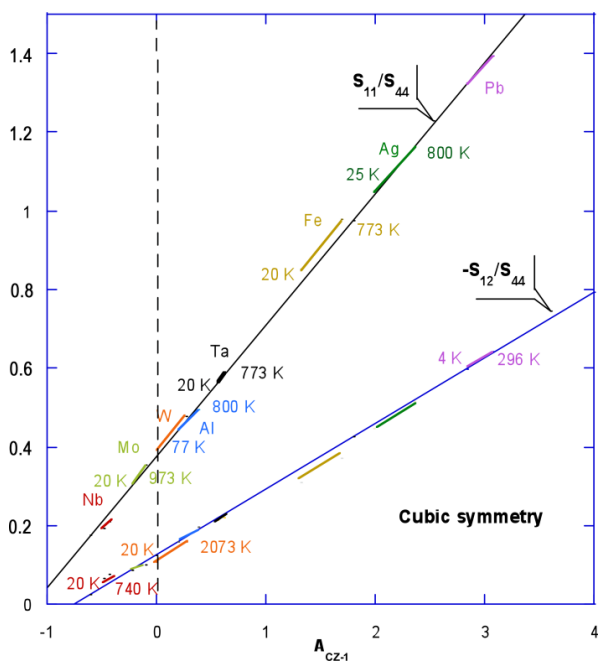


Figure 2.2. *Evolution of elasticity with temperature for fcc and cc metals*

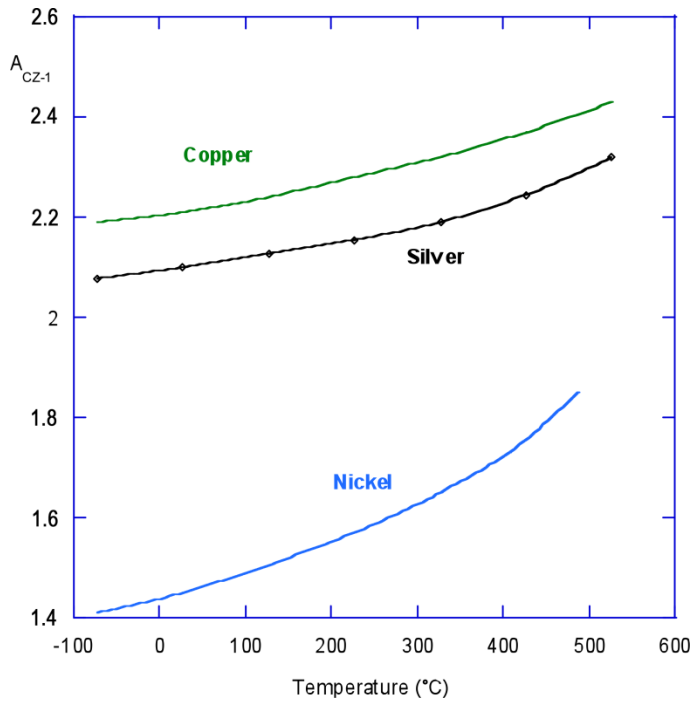


Figure 2.3. Evolution of the anisotropy of several metals with temperature

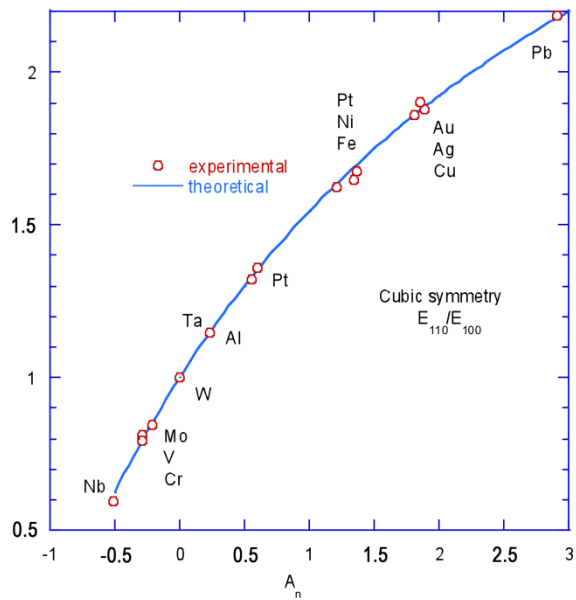


Figure 2.4. Correlation between the experimental ratio of moduli and dimensionless approach

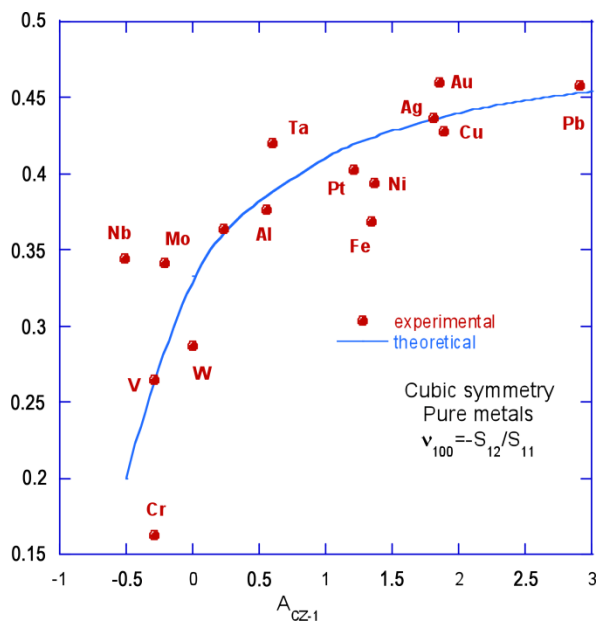


Figure 2.5. *Experimental error on Poisson's ratio*

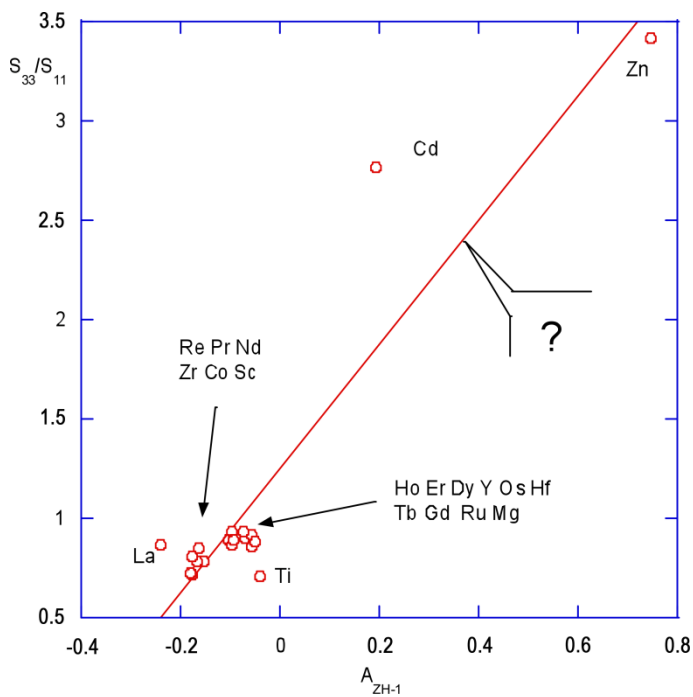
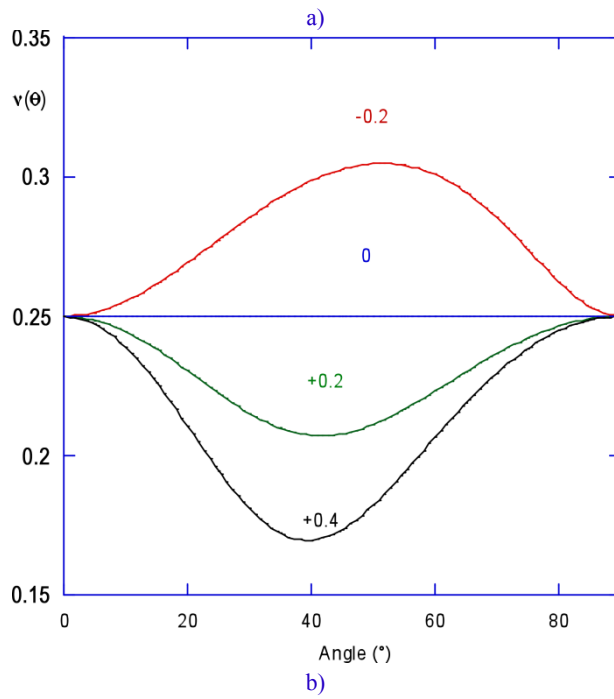
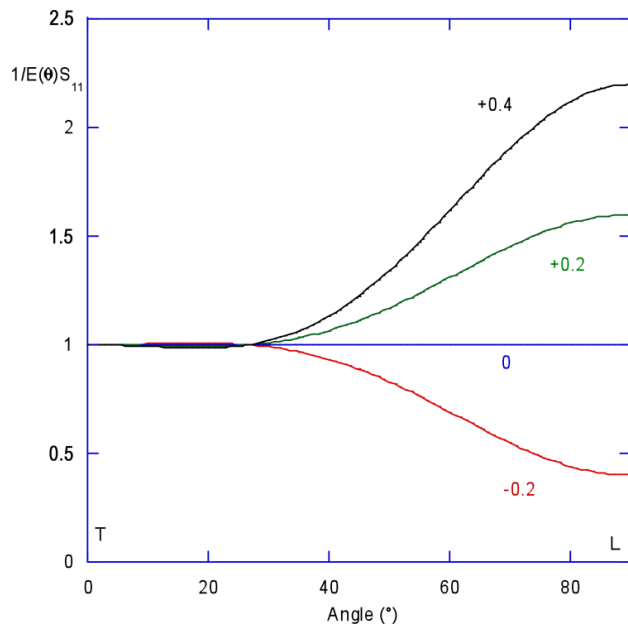


Figure 2.6. *Uncertainty on the dimensionless representation of the elasticity of hexagonal symmetry*



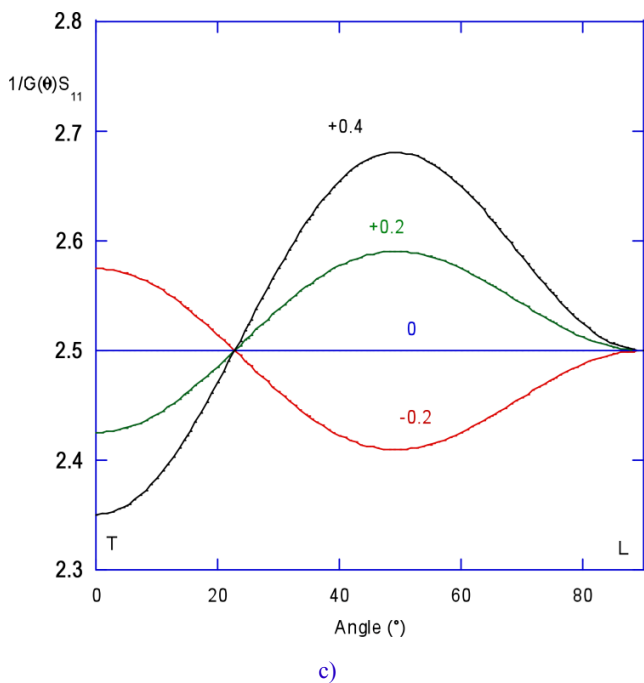


Figure 2.8. Angular representation of the dimensionless elasticity of the hexagonal symmetry: a) Young's modulus, b) Poisson's ratio and c) shear modulus

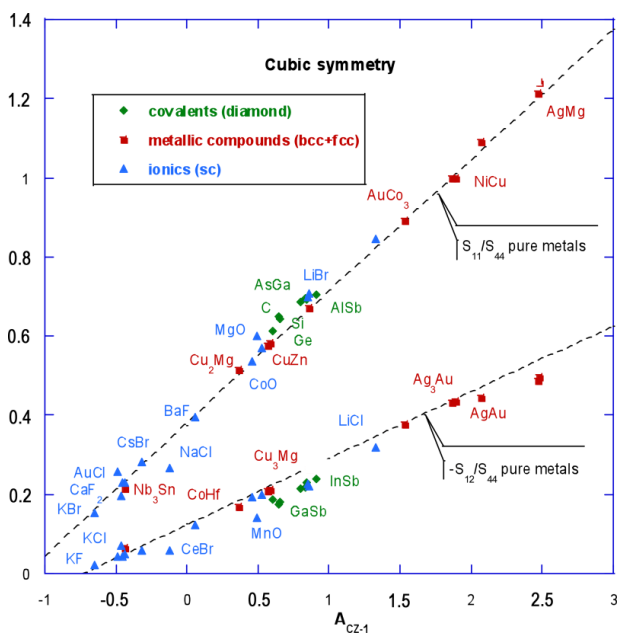


Figure 2.9. Dimensionless representation of the elasticity of all cubic sub-symmetries

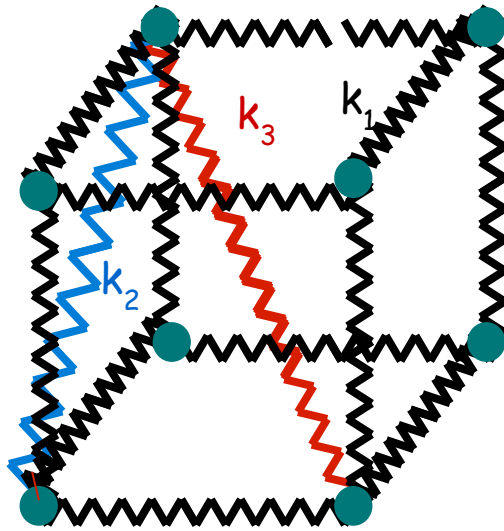


Figure 3.1. Insertion of atomic springs

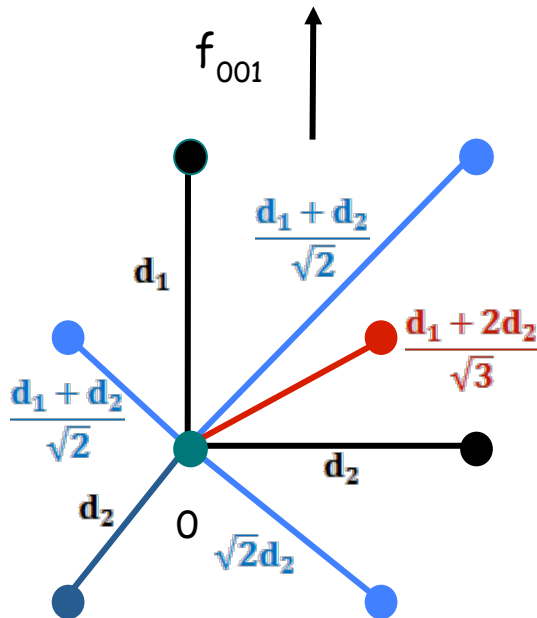


Figure 3.2. Simulation of a traction test on the lattice cell

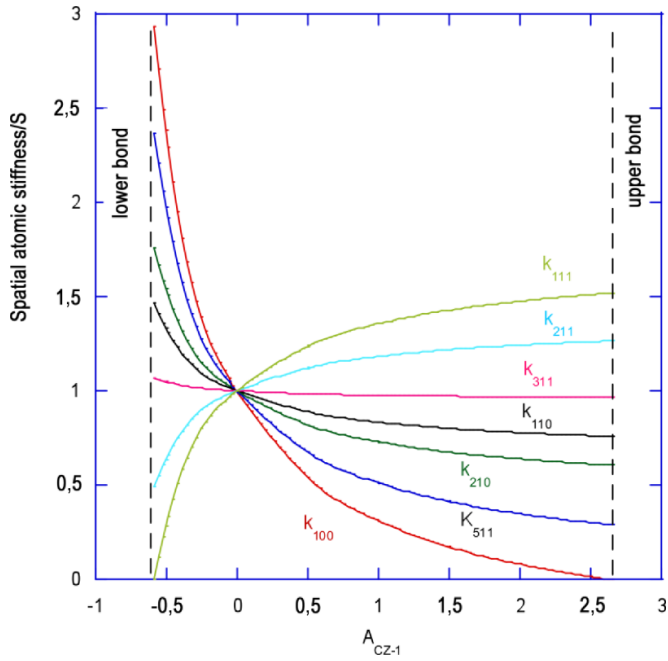


Figure 3.3. *Spatial anisotropy of the representation of dimensionless elasticity at the atomic scale*

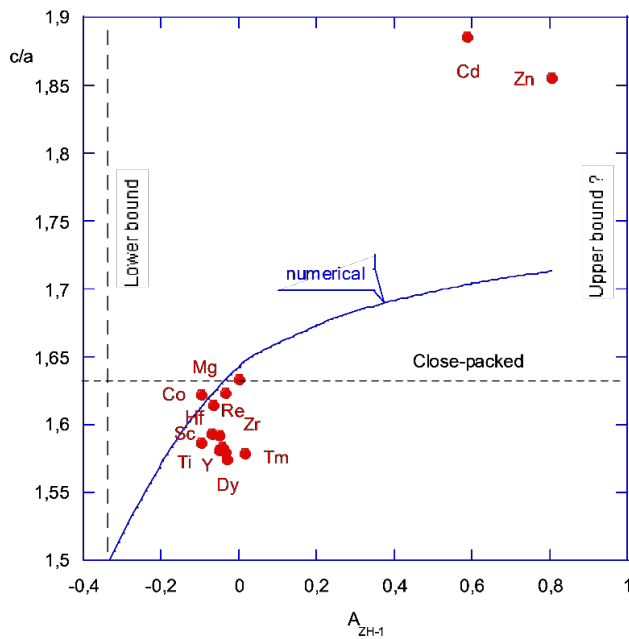


Figure 3.4. *Dependence of c/a ratio on anisotropy (hexagonal symmetry)*

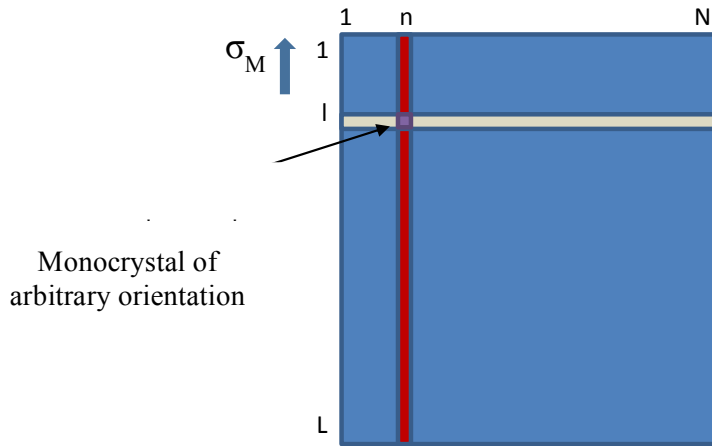
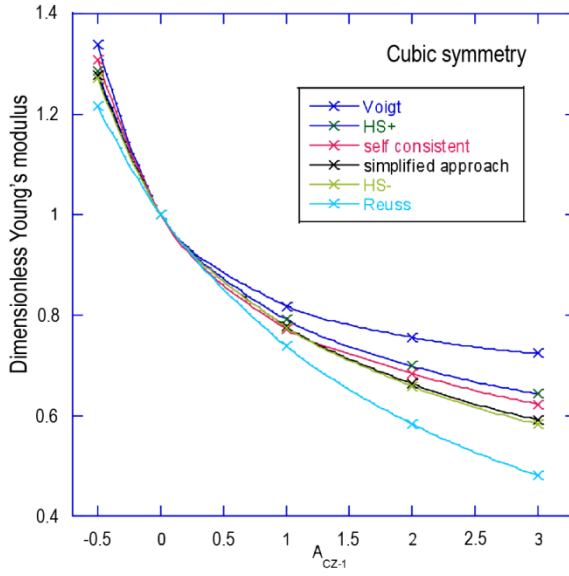


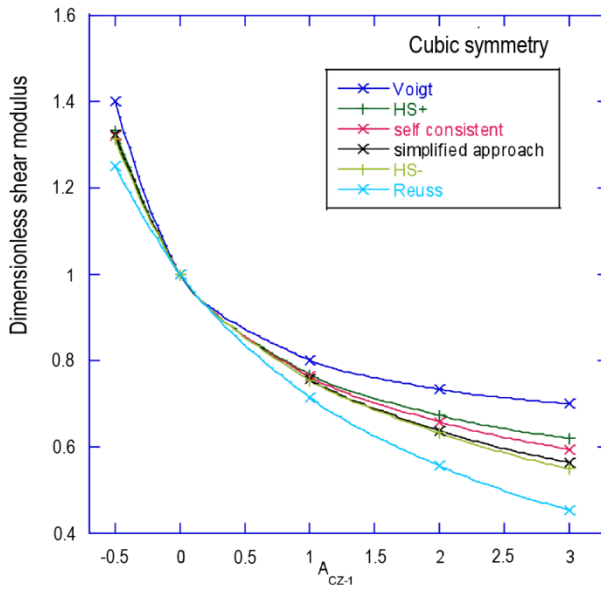
Figure 4.1. Simulation of a traction test on polycrystal

A_{CZ-1}	-0.5	0	1	2	3
S_{11}	3.33	6.0	11.33	16.67	22
S_{44}	16	16	16	16	16
$-S_{12}$	0.67	2	4.67	7.33	10
C_{11}	333.3	250.0	208.2	194.5	187.5
C_{44}	62.5	62.5	62.5	62.5	62.5
C_{12}	83.3	125	145.9	152.7	156.2

Table 4.1. Discrete data of the elasticity of cubic symmetry (C_{ij} in GPa, S_{ij} in TPa^{-1})



a)

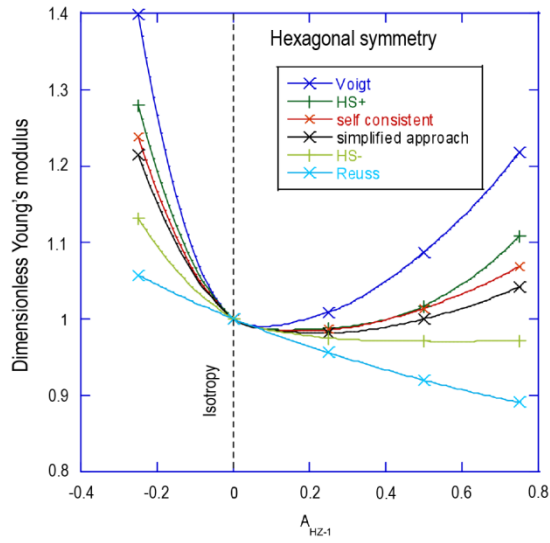


b)

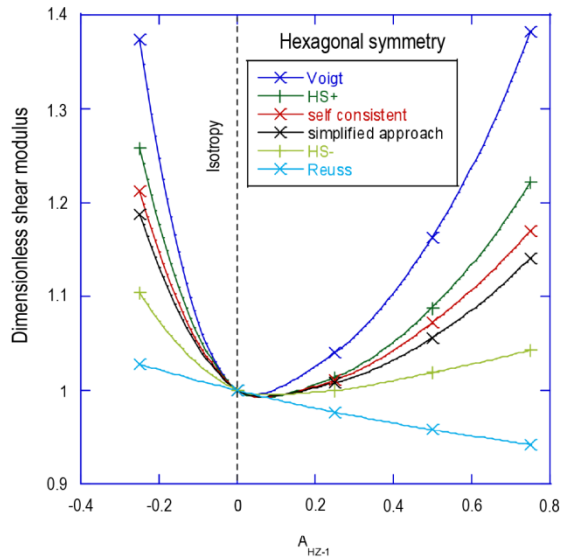
Figure 4.2. Dimensionless representation for the cubic symmetry of the elasticity of a polycrystal: a) Young's modulus and b) shear modulus (Schmitt 2019)

A_{CZ-1}	-0.25	0	0.25	0.5	0.7
S_{11}	6.92	6.4	5.95	5.56	5.22
S_{33}	1.73	6.4	10.42	13.91	17
S_{44}	16	16	16	16	16
$-S_{12}$	3.03	1.6	0.37	-0.7	-1.63
$-S_{13}$	0.43	1.6	2.6	3.48	4.24
C_{11}	186.3	187.5	195.9	213.3	244.8
C_{33}	612.1	187.5	125.2	99.5	85.1
C_{44}	62.5	62.5	62.5	62.5	62.5
C_{12}	85.8	62.5	37.8	7.9	-33.6
C_{13}	68.0	62.5	58.4	55.3	52.8

Table 4.2. *Discrete data of the elasticity of hexagonal symmetry
(C_{ij} in GPa, S_{ij} in TPa^{-1})*



a)



b)

Figure 4.3. Dimensionless representation for the hexagonal symmetry of the elasticity of a polycrystal: a) Young's modulus and b) shear modulus (Schmitt 2019)

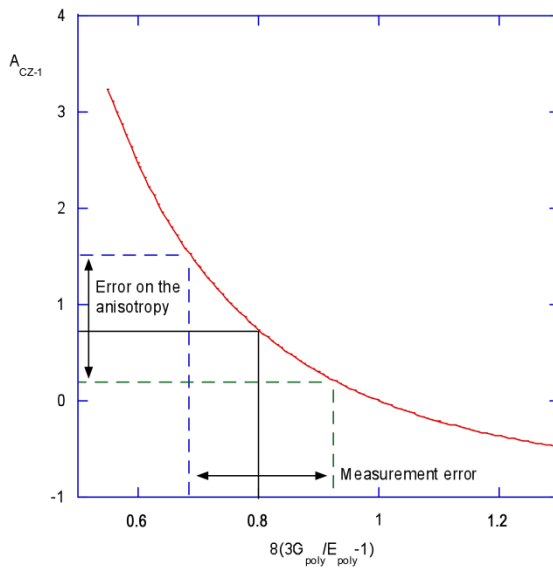


Figure 4.4. Anisotropy determination error related to experimental error measurements on the polycrystal

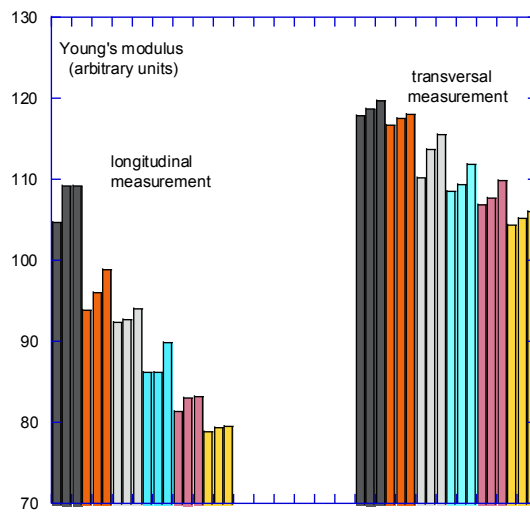


Figure 4.5. Elastic anisotropy of five shades of textured copper alloys

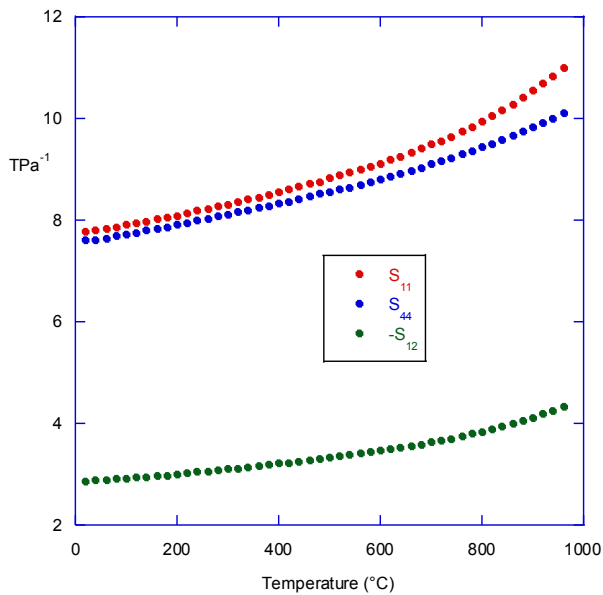


Figure 5.4. Evolution with temperature of the elastic constants of CSMX-4 superalloy

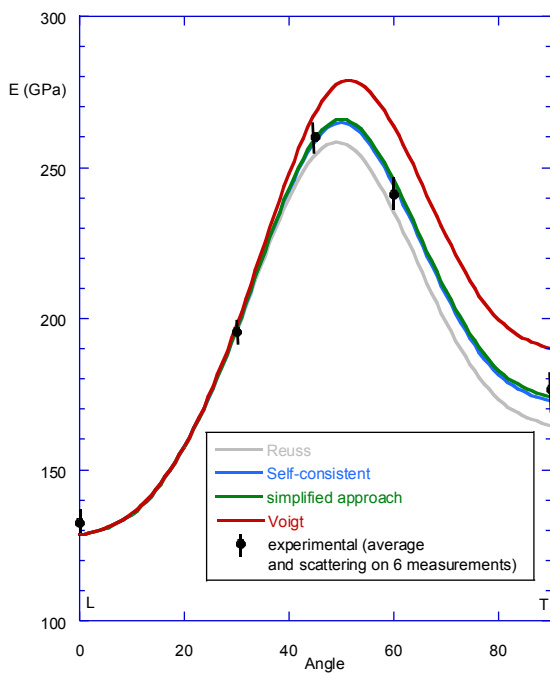


Figure 5.6. Angular elasticity of a superalloy elaborated by directional solidification

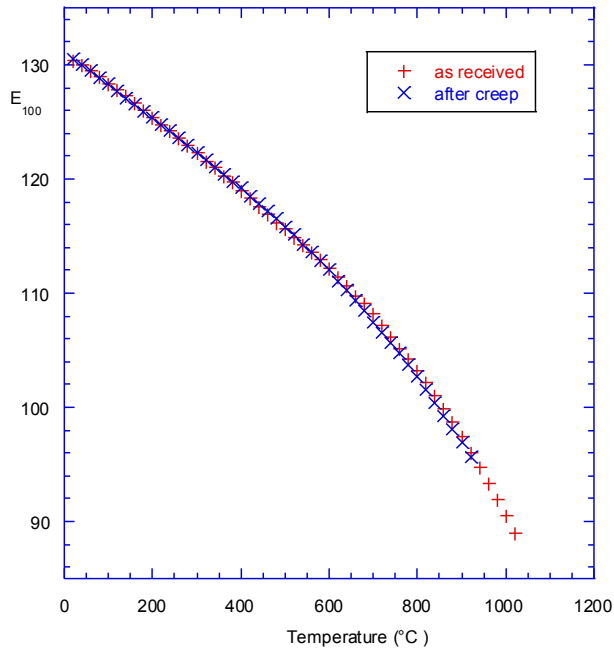


Figure 5.8. Evolution after creep of the elasticity of a single-grained superalloy

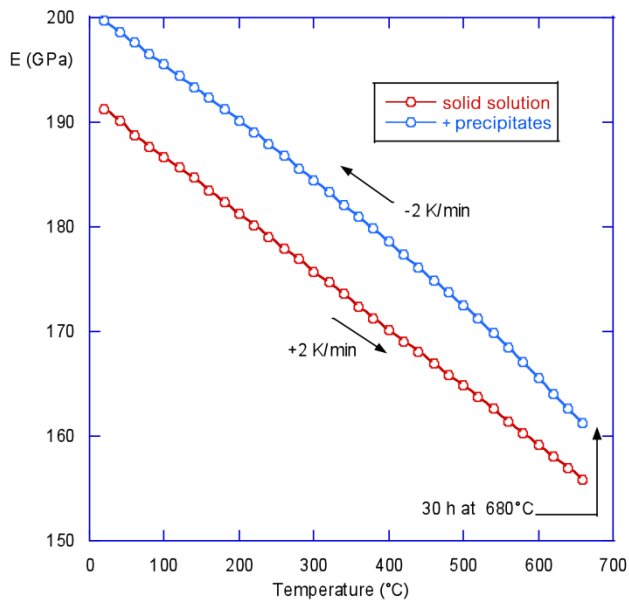


Figure 5.9. Evolution with temperature of the elasticity of an Inconel 718 after precipitation treatment at 680°C

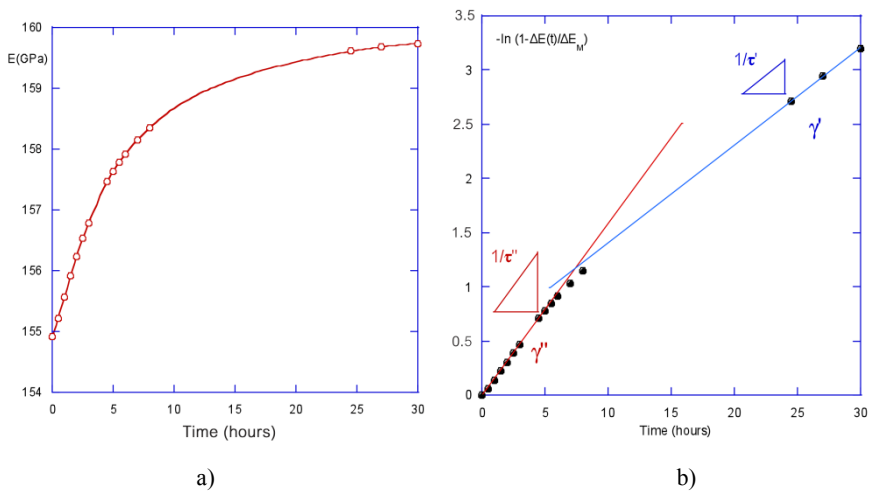


Figure 5.10. Evolution of elasticity in time during the precipitation at 680°. a) Rough representation. b) Analysis based on logarithmic representation

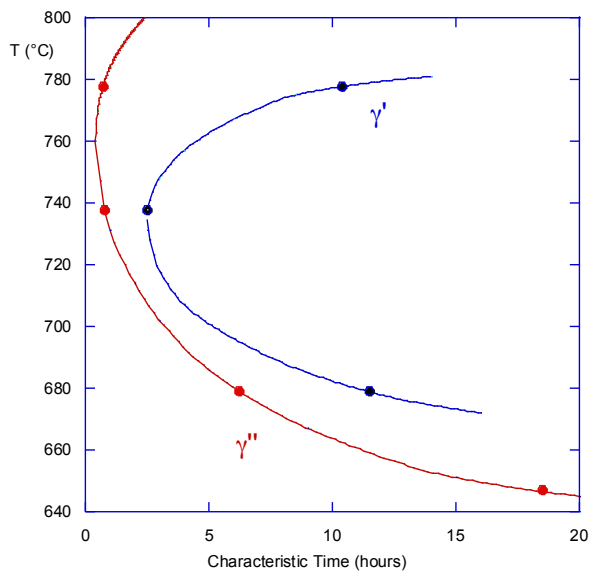


Figure 5.11. TTT diagram of an Inconel 718

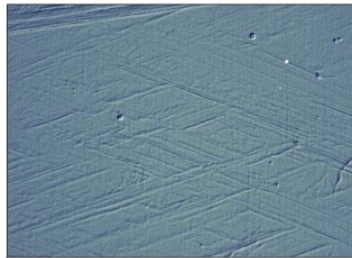
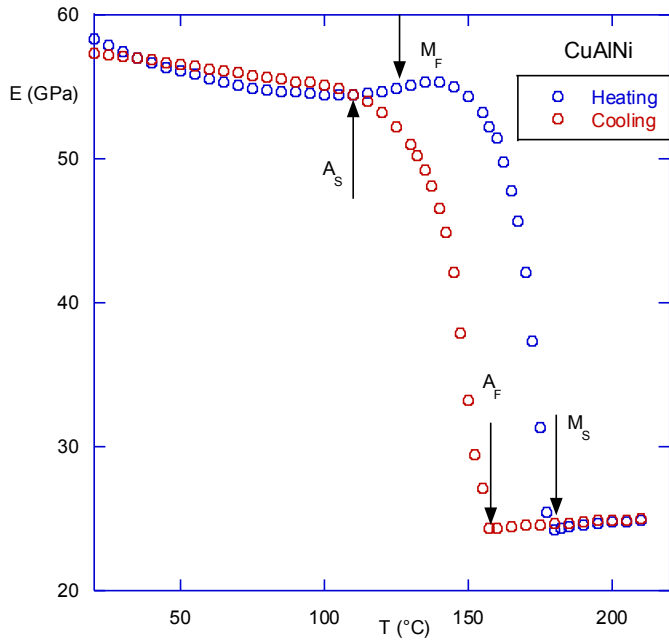
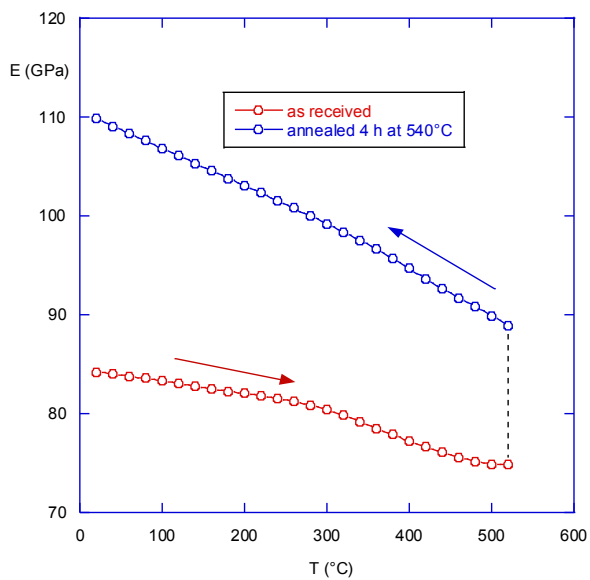
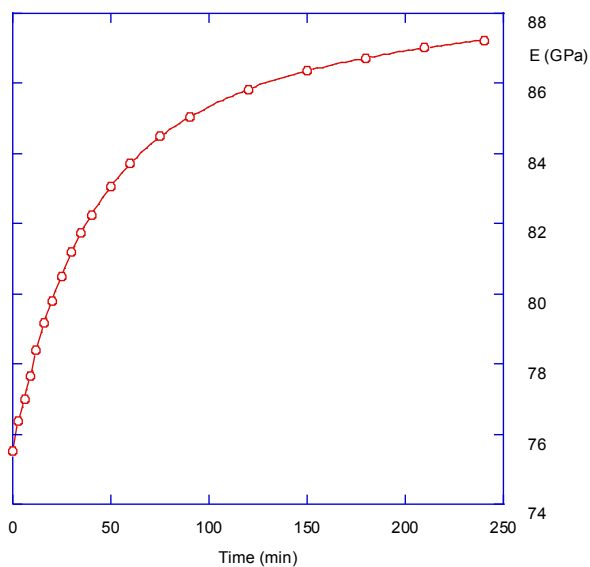


Figure 5.12. Evolution of the elasticity of CuAlNi during its transformation.
Surface observation of martensite variants



a)



b)

Figure 5.13. Phase transformation of a titanium alloy. a) Evolution of elasticity with temperature. b) Kinetics of the transformation

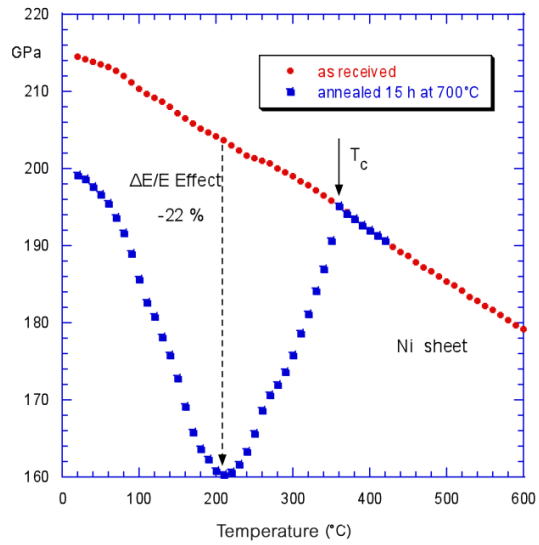


Figure 5.14. Magneto-elastic coupling of pure nickel (Ben Dhia 2016)

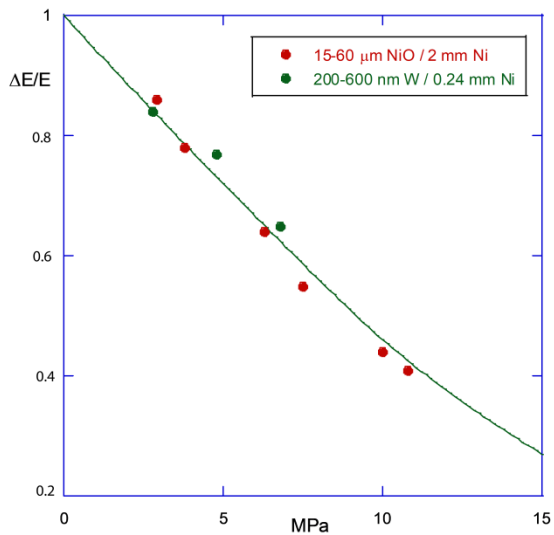


Figure 5.15. Amplitude of ΔE effect as a function of the stress level.
Adapted from Ben Dhia (2016)

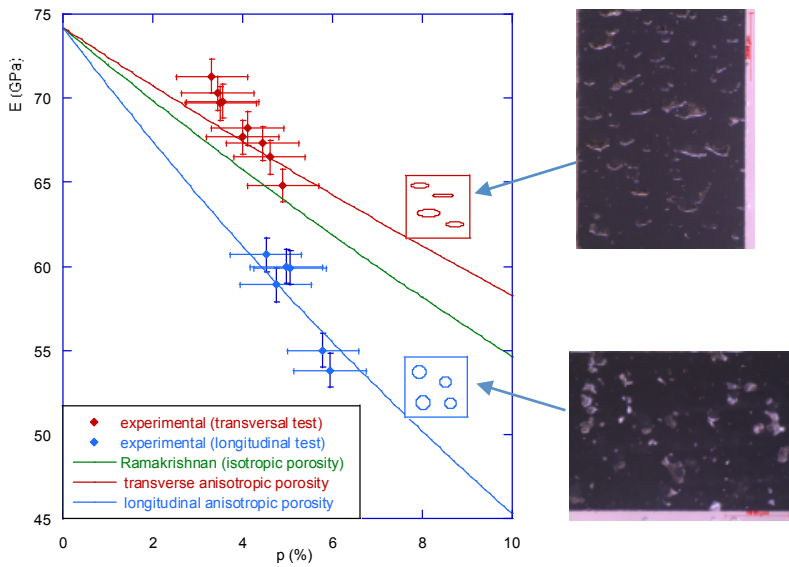


Figure 5.19. Young's modulus of aluminum of additive manufacturing as a function of porosity. Observations of anisotropy of porosity

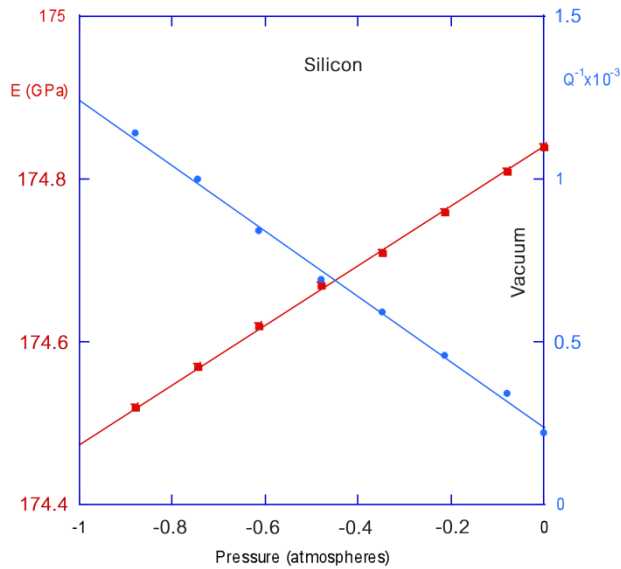


Figure 5.21. Effect of pressure on the Young's modulus and damping of silicon (Ben Dhia 2016)

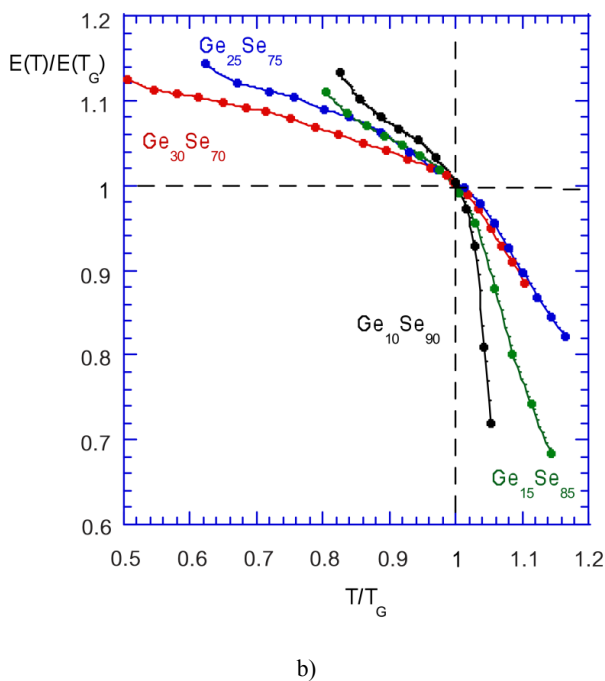
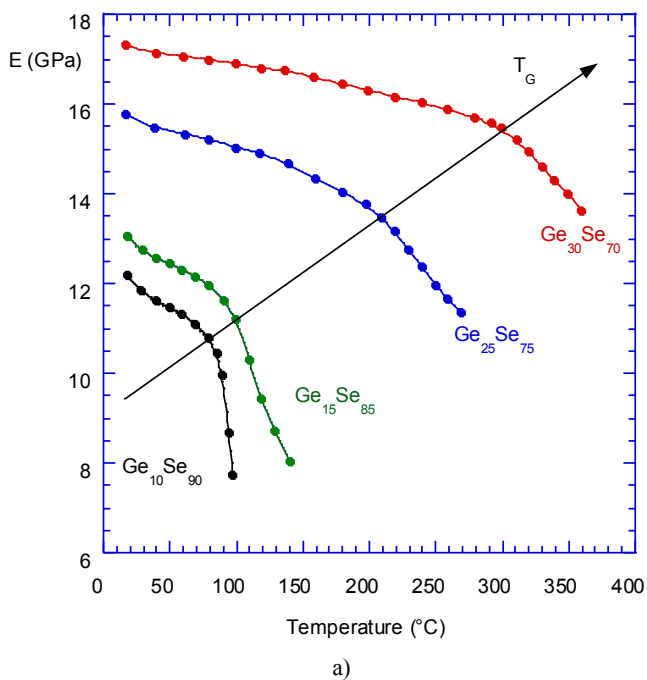


Figure 5.22. Elasticity of SeGe system. a) Rough representation. b) Rationalized representation (Gadaud and Pautrot 2003)

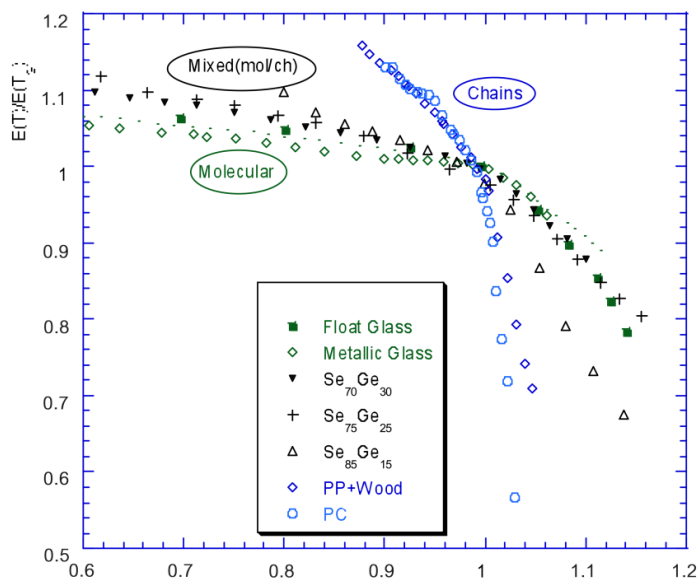


Figure 5.23. Dimensionless elasticity of amorphous materials

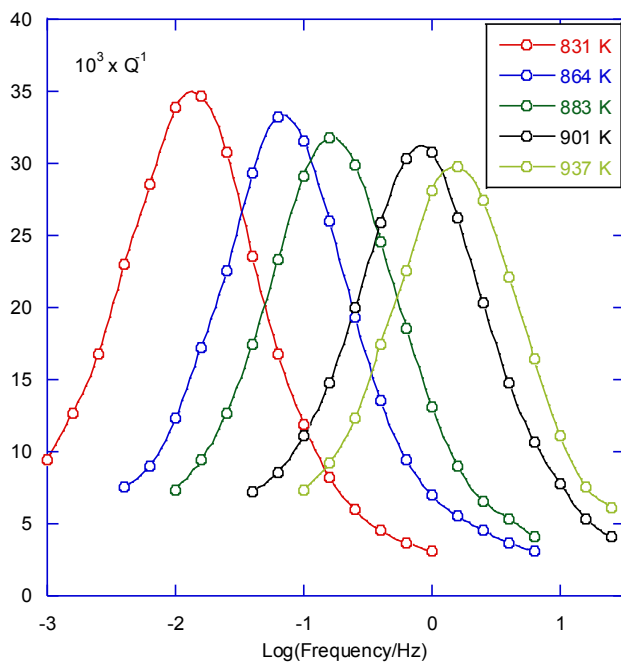


Figure 5.24. Isothermal damping spectra of a γ' - Ni_3Al polycrystal (Gadaud and Chakib 1993)

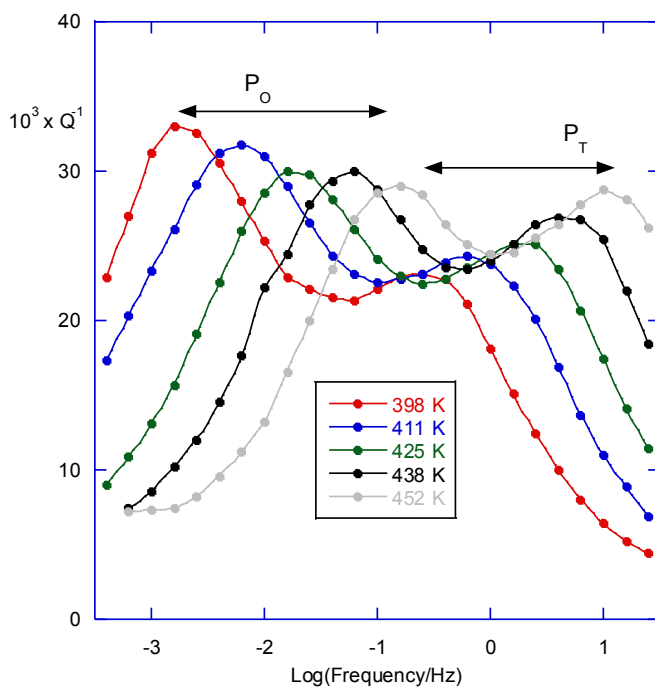


Figure 5.26. Isothermal damping spectra of YBCO superconductor (Gadaud and Kaya 1994)

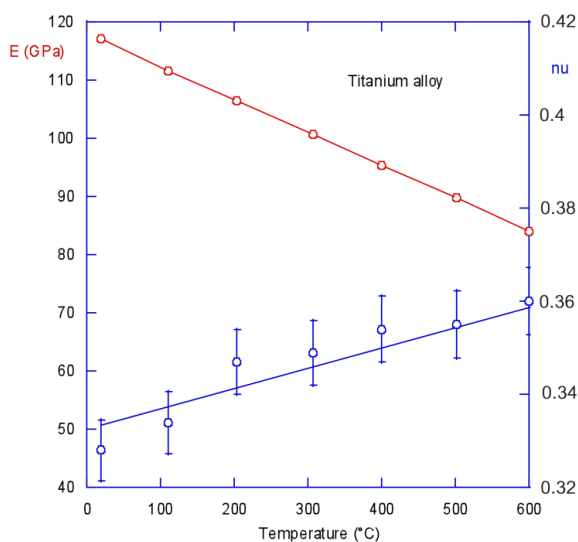


Figure 6.1. Elasticity as a function of temperature for an isotropic titanium alloy. Tension-compression test

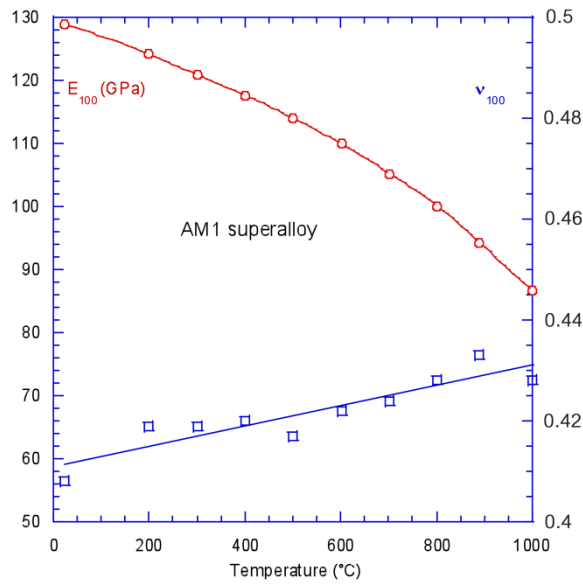


Figure 6.2. Elasticity as a function of temperature for an anisotropic superalloy. Tension–compression test along a $\langle 100 \rangle$ direction

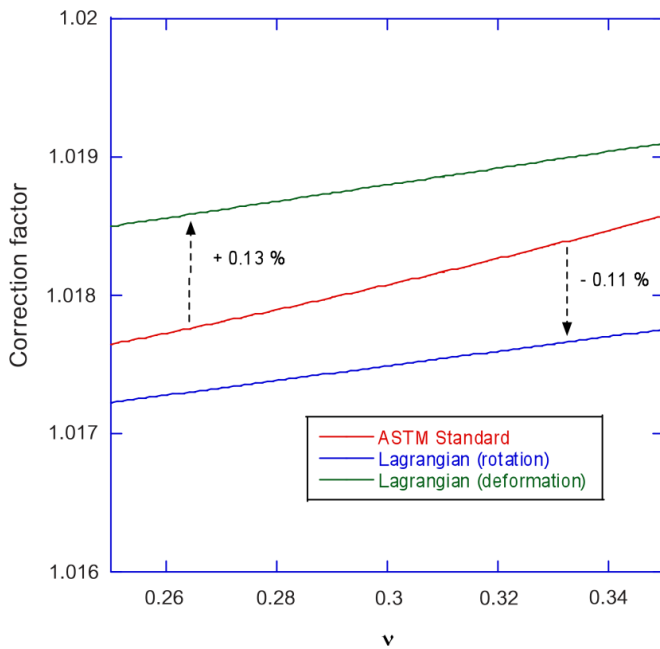


Figure 7.1. Relative variation of the Young's modulus measured during bending by taking into account the shear by various approaches

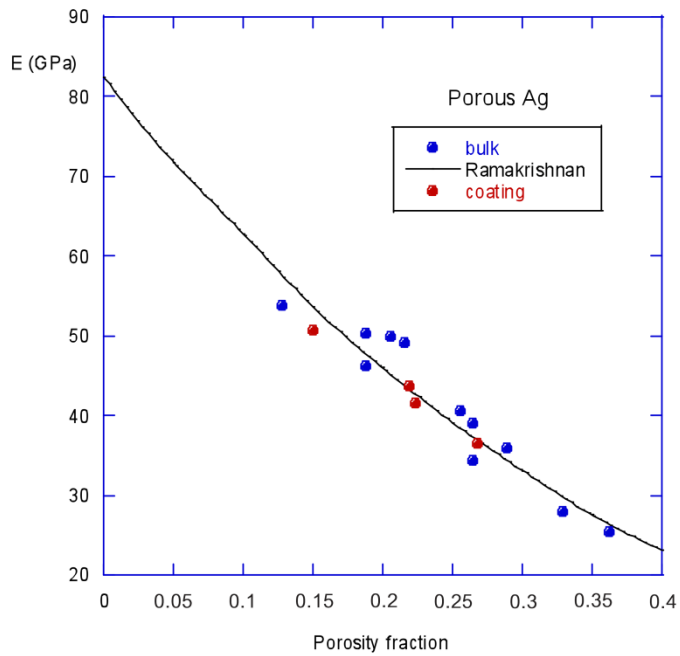


Figure 7.3. Comparison of the elasticity of porous silver under massive form or as coating (Caccuri et al. 2014)

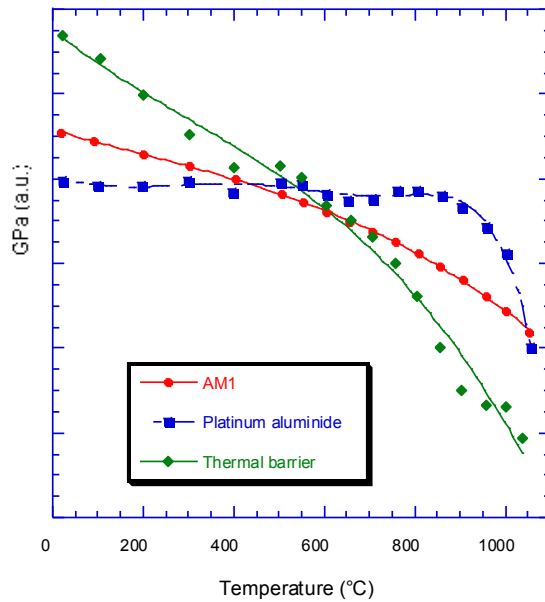


Figure 7.6. Elasticity with temperature of the superalloy + anticorrosive platinum aluminide + thermal barrier (Gadaud 2015)

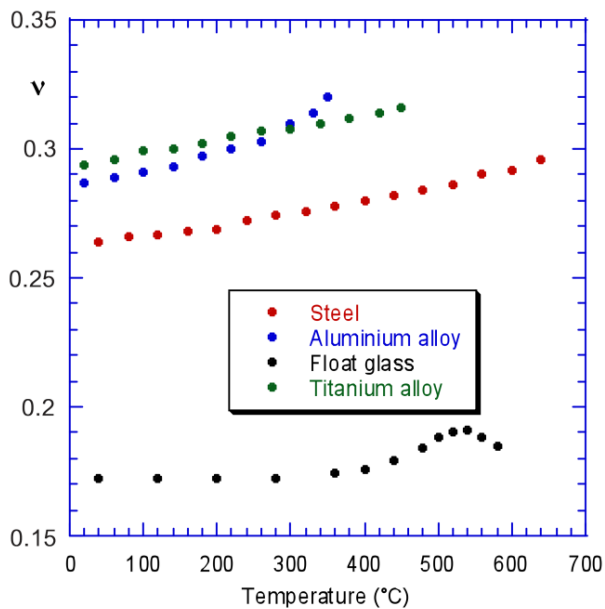


Figure 8.2. Evolution of Poisson's ratio with temperature for various materials (Gadaud et al. 2009)

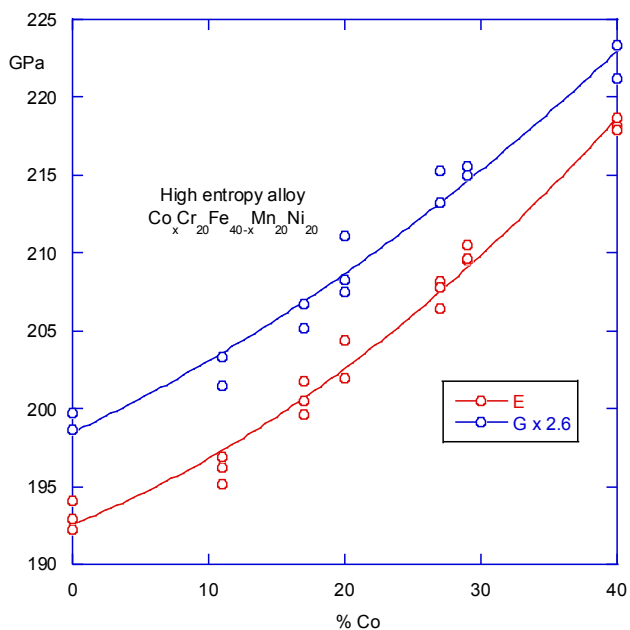


Figure 8.3. Evolution with temperature of Young's and shear moduli for a high-entropy alloy

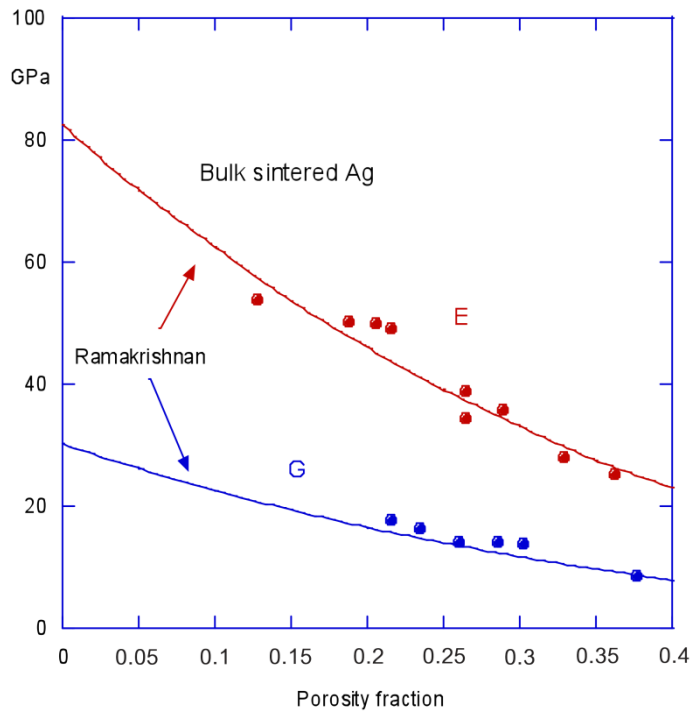


Figure 8.4. Evolution with temperature of Young's and shear moduli of porous bulk silver (Caccuri et al. 2014)

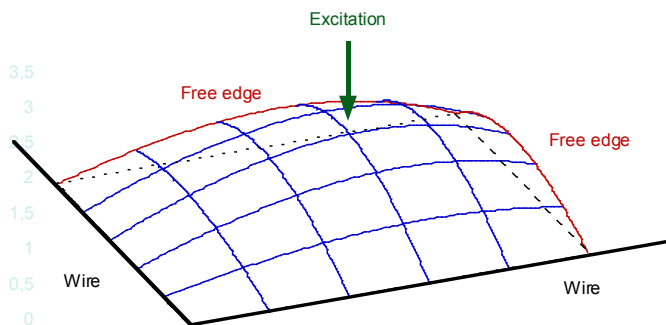


Figure 9.1. Vibration mode on a quarter of the plate

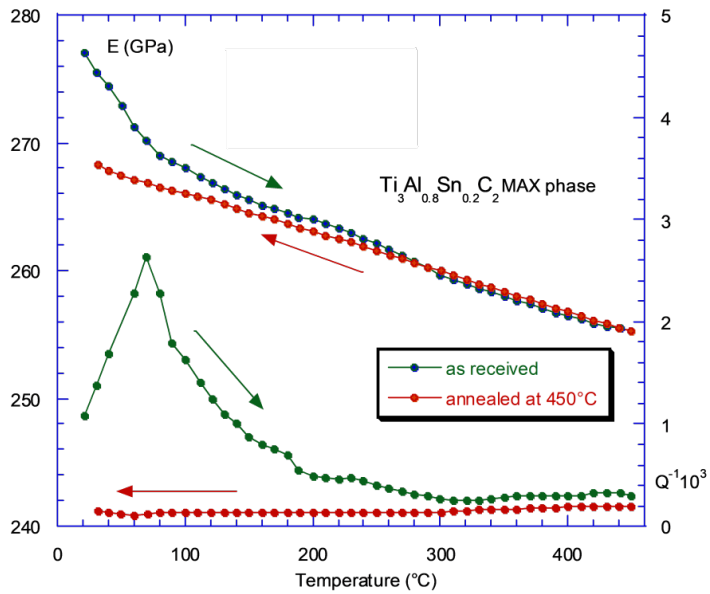


Figure 10.1. Evidence of the relaxation of elaboration stresses for an HIP sintered MAX phase. Adapted from Gadaud and Pautrot (2012)

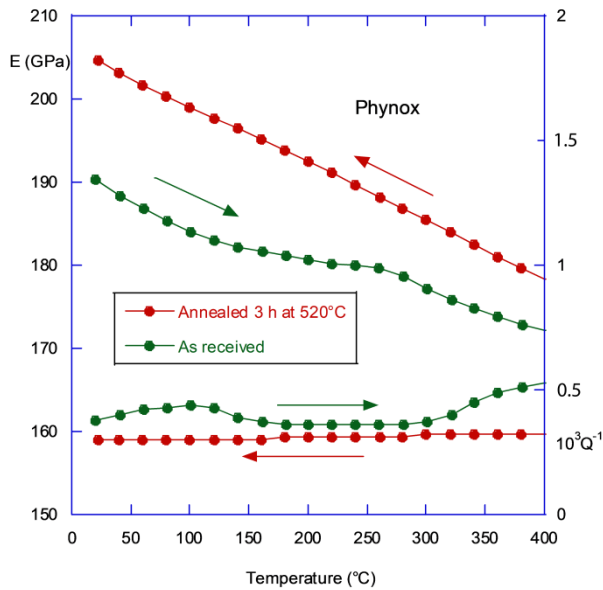


Figure 10.2. Evidence of the relaxation of elaboration stresses for rolled steel. Adapted from Gadaud and Pautrot (2012)

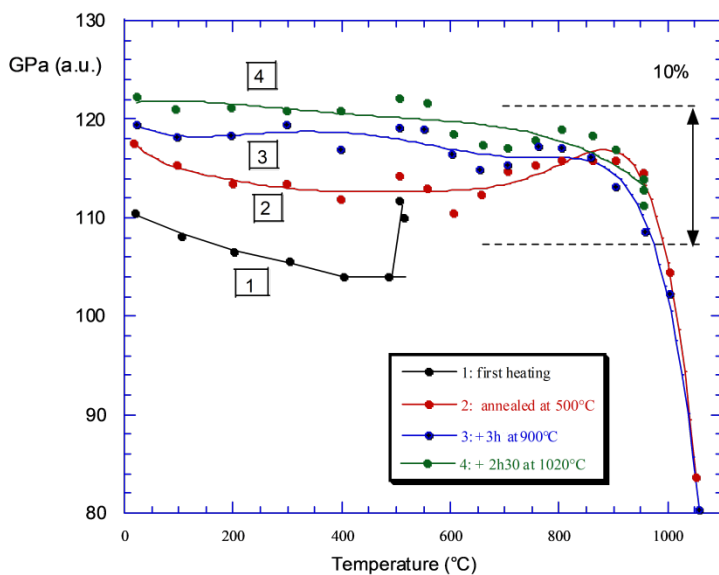


Figure 10.3. Evidence of the relaxation of elaboration stresses of AlPtNi coating during heat treatment. Adapted from Gadaud and Pautrot (2012)

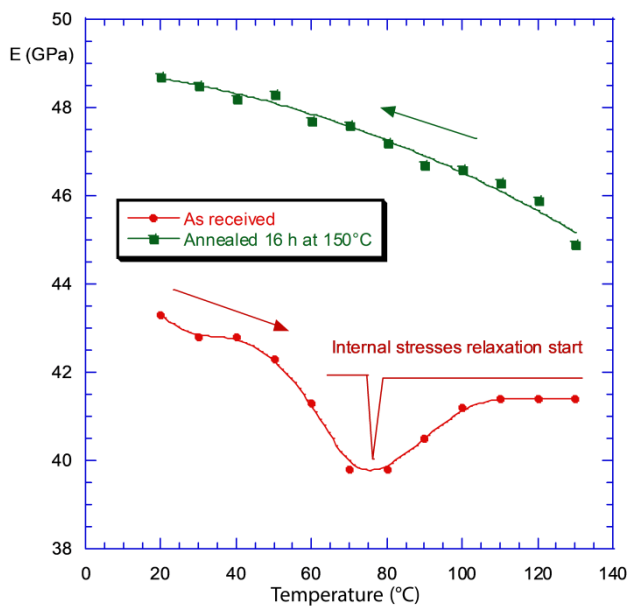


Figure 10.4. Evidence of the relaxation of elaboration stresses of a porous silver coating during thermal treatment. Adapted from Cacurri et al. (2014)